THESIS FOR THE DEGREE OF DOCTOR OF PHILOSOPHY

Microstructure Development of WC-Co Based Cemented Carbides During Creep Testing

AMINE YOUSFI

Department of Physics
CHALMERS UNIVERSITY OF TECHNOLOGY
Göteborg, Sweden 2016

Cover:

Bright field TEM micrograph of a fine-grained Cr-doped material crept at 1000 °C

To my grandparents Yousfi Loucif and Saliha

Microstructure Development of WC-Co Based Cemented Carbides During Creep Testing

Amine Yousfi

Department of Physics

Chalmers University of Technology

Abstract

The aim of this work is to understand the mechanisms behind the plastic deformation of WC-Co based cemented carbides. The microstructure of two series with different WC grain size was investigated before and after creep deformation using quantitative microscopy, atom probe tomography, and transmission electron microscopy. The first series consisted of two WC-Co based cemented carbides with fine WC grain size used for machining applications, an un-doped WC-Co material with 10 vol % binder phase and a Cr-doped WC-Co material with a higher fraction of binder phase, 16 vol %. The second series consisted of two WC-Co based cemented carbides with coarser WC grain size used for mining applications, an un-doped and a Cr-doped WC-Co based materials. In both materials, the binder phase represented 10 vol% of the total volume. High temperature compressive creep tests were performed under a stress of 900 MPa at 900, 1000 and 1100 °C and 300 MPa at 1100 °C, and the test bars were deformed to different strains. A heat treatment was also performed at 1000 °C in order to see the effect of an applied load on WC grain growth.

Preferential WC grain growth perpendicular to the applied load was found to occur during creep deformation at 1000 and 1100 °C. WC grains in the crept materials had a significantly increased dislocation density, with a large number of dislocation lines merging on the grain surfaces. It is suggested that merging matrix dislocations having a screw component may act as nucleation points to grow new layers of W and C. The binder phase grains became, on the other hand, smaller during creep deformation at 1000 °C, and lost their finger-like morphology. This may be explained by binder phase grain rotation caused by dislocation glide. The crept microstructures had an increased number of density of WC/WC grain boundaries infiltrated by the binder phase. This suggests that grain boundary sliding occurred, accommodated by binder phase infiltration. Some WC grain surfaces facing the infiltrated grain boundaries had a step surface of an angle of 90 and 120 °. The atoms at the surface were rearranged to reduce the surface energy. Intergranular cavities were also formed during creep deformation. This cavity formation indicates that also unaccommodated grain boundary sliding took place during creep deformation.

APT revealed a variation in the concentration of W and C in the binder phase, and that the solubility of W and C increased with increase of temperature. The rapid cooling from the creep test temperature ensures that the composition of the binder phase in crept materials represents the composition during the test. WC/binder phase boundaries of the as-sintered fine grained Cr-doped material showed an enrichment in Cr at the phase boundary and formation of thin (Cr, W) carbide layer on the surface of WC grains at the phase boundary. This (Cr, W) carbide layer seems to disappear when the material is heat treated at 1000 °C. The thermodynamic calculations found that this cubic layer is stable below 940 °C when no M_7C_3 carbides are formed.

Preface

The research work presented in this thesis was carried out in the Division of Materials Microstructure at the Department of Physics, Chalmers University of Technology, Gothenburg, Sweden, during the period October 2011 to May 2016, under supervision of Professor Lena Falk and co-supervision of Professor Hans-Olof Andrén.

List of appended papers

I. *Evolution of the microstructure during creep testing of WC-Co based cemented carbide*
M. A. Yousfi, A. Nordgren, L. K. L. Falk, H.-O. Andrén
Proceedings of the 18th Plansee Seminar, HM58 (2013) 1467-1475

II. *Deformation mechanisms in a WC-Co based cemented carbide during creep*
M. A. Yousfi, J. Weidow, A. Nordgren, L. K. L. Falk, H.-O. Andrén
International Journal of Refractory Metals and Hard Materials, 49 (2015) 81-87

III. *The creep behaviour of un-doped and Cr-doped WC-Co cemented carbide materials*
M. A. Yousfi, A. Nordgren, S. Norgren, H.-O. Andrén, L. K. L. Falk
Manuscript for submission to Int. Journal of Refractory Metals and Hard Materials.

IV. *Atom probe analysis of the binder phase and phase boundaries in un-doped and Cr-doped WC-Co cemented carbides*
M. A. Yousfi, H.-O. Andrén, L. K. L. Falk
In manuscript

V. *The effect of WC grain size on the creep behaviour of WC-Co cemented carbides*
M. A. Yousfi, H.-O. Andrén, L. K. L. Falk
In manuscript

My contribution to the appended papers

Paper I

I prepared the specimens for microscopy (including cutting, mechanical grinding and polishing, ion polishing) using the CMAL equipment. I characterized the material using SEM and EBSD. I wrote the first draft of the paper, and I was the first author.

Paper II

I prepared all the specimens for electron microscopy (including cutting, mechanical grinding and polishing, ion polishing) using the CMAL equipment. I characterized the material using SEM and TEM. I wrote the first draft of the paper, and I was the first author.

Paper III

I prepared all the specimens for microscopy (including cutting, mechanical grinding and polishing, ion polishing), and characterized the material with SEM using the CMAL equipment. I characterized the presence of M_7C_3 together with Martin Schwind at Seco Tools AB. I wrote the first draft of the paper, and I was the first author.

Paper IV

I prepared all the specimens for APT (including cutting, electropolishing, ion milling with the FIB/SEM) using the CMAL equipment. I analysed the specimens with APT and analysed the data with IVAS. I wrote the first draft of the paper, and I was the first author.

Paper V

I prepared all the specimens for electron microscopy (including cutting, mechanical grinding and polishing, ion polishing) using the CMAL equipment. I characterized the materials with SEM and TEM. I co-authored the manuscript together with my supervisors.

Contents

x

Chapter 1. Introduction

Cemented carbides are sintered hard materials with exceptional mechanical properties that make them commercially useful in machining operations such as turning, milling, and drilling, and also in mining, and metal forming operations [1]. Cemented carbide materials have a microstructure that consists of hard refractory carbides embedded in a ductile metal matrix, which gives them their unique properties. Since the early 20th century, the cemented carbides have been widely used in many manufacturing processes that benefit from their combination of high hardness, fracture toughness, strength, and wear resistance. During sintering, many parameters such as temperature, holding time and carbon level are controlled in order to reach the desired properties. WC grain growth takes place during sintering, thus changing the material properties [2,3]. Grain growth inhibitors such as V or Cr are therefore added to the raw powder during milling. These inhibitors are found to dissolve in the binder phase and also segregate to the grain and phase boundaries [4,5]. It has also been pointed out that WC grains are interconnected to form a continuous skeleton. But Co is also found to segregate to the WC/WC grain boundaries with 0.5 to 1 monolayer [5–8].

During operation the tool material is exposed to high loads and high temperatures. Usually, a wear resistant ceramic coating is deposited onto the cemented carbide tool surface by chemical or physical vapour deposition. As a result, the tool life under severe cutting conditions is often limited by plastic deformation of the cemented carbide [9]. Big efforts are put to improve the properties of these composite materials at high temperature but the deformation mechanisms are not well understood. It was originally explained that cemented carbides behave like ceramics and tend to fracture when they are subjected to mechanical loads at low temperatures [10]. When the temperature is increased, the deformation mainly takes place in the metallic binder phase [11,12]. Later, it was confirmed that cemented carbides have a brittle behaviour at temperatures up to around 600 °C [13,14]. Different phenomena associated with plastic deformation of cemented carbides have, thus, been observed at higher temperatures. The controlling mechanisms are, however, not understood.

1.1 Aim

This research was undertaken in order to identify the deformation mechanisms associated with the compressive creep behaviour of WC-Co cemented carbides. The purpose was to deform the material in a controlled way, and to investigate the microstructure of the material before and after the deformation.

Chapter 2 – Cemented carbides

The history of cemented carbides dates back to the end of the 19th century and has been described in a review paper by H. Exner [1]. H. Moissan, in 1896, was the first person able to produce W_2C by using an electric furnace. P. Williams, who was a colleague of H. Moissan, succeeded to produce the monocarbide, WC, two years after. Since the material was considered too brittle, no practical application could be found. The material was improved with time by introducing hot pressing for compaction of the carbides. It was not until 1922 that the first hardmetals were invented by F. Skaupy and H. Baumhauer from Osram Company by infiltrating the carbides with metals like Fe, Ni, and Co. Then K. Schröter found that Co was the best alternative to use as binder phase [15]. The product was first called WIDIA (an acronym for "wie Diamant"), which means "like diamond" in German. By the end of the 1920's and beginning of the 1930's, cemented carbides with additions of cubic carbides were presented [1,10].

2.1 Fabrication

WC-Co based cemented carbide is a typical product of powder metallurgy. The material is fabricated from WC powder, high purity cobalt powder, and possibly also other additives. The main steps in the fabrication procedure are milling of the starting powder mixture, drying of the powder slurry, forming of a green body and sintering. These steps are described in the following sections.

2.1.1 Powder production

There are different ways to obtain the WC powder. The traditional way is the reduction of the oxide WO_3 followed by carburisation. Direct carburisation of tungsten oxides can also be conducted [16]. WC powder particles are polycrystalline for particle sizes larger than 2 μm and essentially monocrystalline for smaller sizes [17].

2.1.2 Milling

The milling process aims at eliminating agglomerates of powder particles and giving a homogeneous mixture and a better spread of the WC grains in the binder. The size of the

powder particles can be controlled to some extent during milling, since the powder particles are reduced in size during milling. WC, Co, and other additive powders are mixed and milled by ball milling in stainless steel vessels. Usually a 5:1 ratio in weight between milling balls and powder is used. The balls are called Cylpebs and are made of WC-Co. Carbon is also added during milling in order to compensate for the loss in C that will happen during sintering. It is important to control the level of C in order to avoid formation of eta phase (M_6C) or graphite, which are harmful to the toughness of the material, see the phase diagram in Figure 2.1. Alcohol is used as milling liquid and binding wax is also added in order to strengthen the green body [18]. The green body is the powder compact that is densified during sintering.
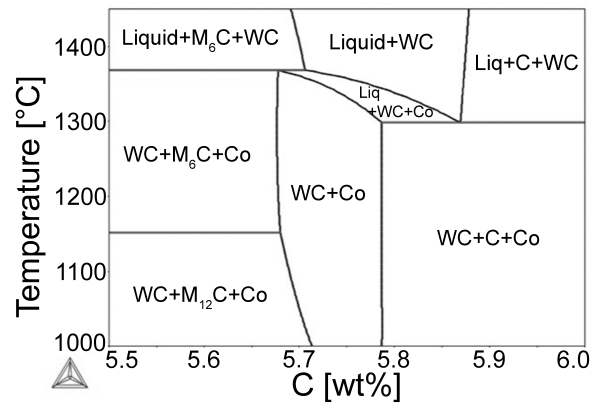

Figure 2.1: Phase diagram of the W-C-Co system with 10 wt% Co [19].

2.1.3 Drying

After milling, the powder slurry is dried from milling fluids. In industry, this is achieved through the spray drying process. The milled powder suspension is sprayed into a chamber through an atomiser using a nitrogen gas stream at 200 °C. The alcohol will then evaporate, and granules with a spherical shape are formed due to surface tension forces.

2.1.4 Pressing

The granules are pressed into shape using rigid steel or carbide dies and pressures of up to 150–990 MPa [19,20]. Components can be pressed directly into specified shapes or they may be pressed into large blocks, which will later be shaped by machining and grinding. Different methods for pressing the granules are used. One of the methods is called uniaxial pressing. It consists of a rigid die in which an upper and a lower punch are inserted. The die is filled with granules and they are compacted by the compression of the two punches. Another method, the one that was used for the preparation of the material in this study, is isostatic pressing. The

4

dried granules are placed in rubber bags that are sealed and then inserted into a liquid, e. g. water. The water is pumped to very high pressure. A large variety of geometries can be shaped with this method. A third method that could be used is powder injection moulding method (PIM). The technique is derived from the plastic injection moulding. This method is very economical for mass production of components that are difficult to shape or machine by conventional methods.

The pressing of the granules results in the formation of a green body. It consists of the powder particles linked by the binder wax, and has a relatively high porosity. The shape of the green body is similar to that of the final component, but larger in size because of shrinkage of the component that occurs during sintering. It is important to use the right pressing method depending on the desired shape of the component, in order to get a homogeneous compaction.
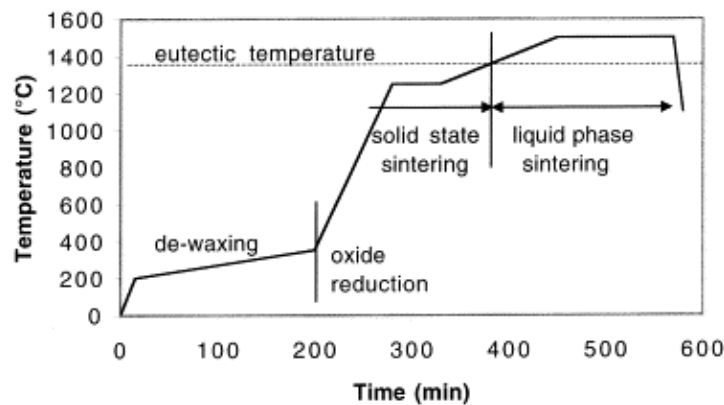
2.1.5 Sintering

Figure 2.2: Time–temperature cycle for sintering of cemented carbides [21].

The aim of sintering is to densify the green body, remove the binding wax, and bind the powder grains, as this will increase the strength of the component. The porosity will be removed and the component will obtain its final dimensions. The temperature–time programme for sintering of cemented carbide green bodies may be divided into several steps, see Figure 2.2. First there is de-waxing and de-gassing of the binders which starts at 200–300 °C, then the oxide reduction follows right after de-gassing until 1000–1100 °C, which is the temperature where solid state sintering starts [21,22]. At this stage surface diffusion and bulk transport occur [23]. This results in a decreased porosity and gives a first shrinkage of the component. This stage continues with increasing temperature until it reaches the melting point of the binder phase constituents at approximately 1300–1350 °C depending on the added elements (see the phase diagram in Figure 2.1). Above that temperature, liquid phase sintering starts. During this stage, small WC grains are dissolved in the binder due to their high surface energy. If the binder phase is not saturated, larger WC grains will also start to dissolve. Once

the binder is saturated, the WC dissolved in the binder will re-precipitate on WC grains, usually the largest grains. This process is called Ostwald ripening. The re-precipitation will continue during cooling of the component, this time in solid state sintering. Additional grain growth will occur during this stage. Most of the W and C will be re-precipitated, but a few atomic % will remain dissolved in the binder after cooling [5].

2.2 Microstructure

The microstructure of cemented carbide is important as it determines the properties of the material. Depending on the powder particle size and size distribution, the composition, and the sintering process, the grain morphology and grain size of the sintered material may vary significantly. Different parameters in the fabrication process will have a direct effect on the evolution of the microstructure. The microstructure of a WC-Co based cemented carbide doped with Cr is shown in Figure 2.3. WC grains appear with bright contrast and form a continuous skeleton, while the Co-rich binder phase that cements the WC grains appears with dark contrast.
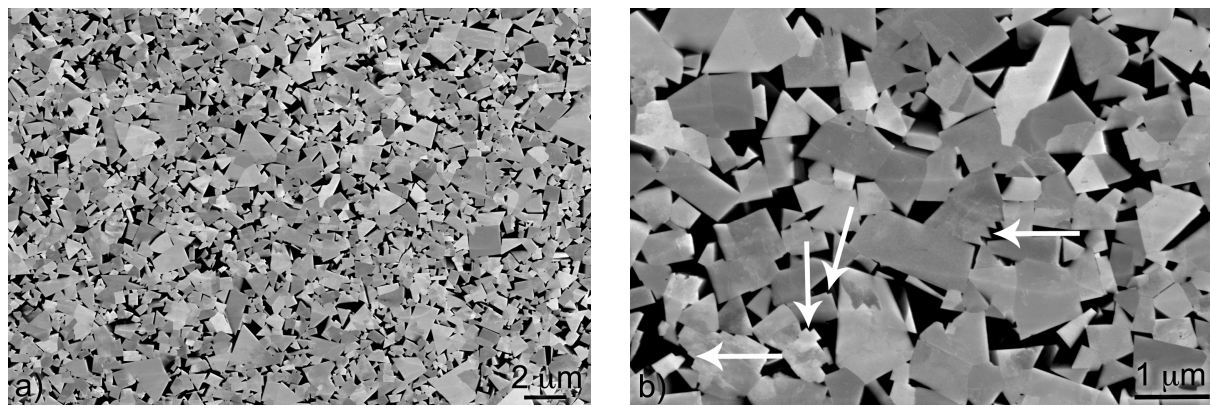

Figure 2.3: The general microstructure of a WC-Co cemented carbide material doped with Cr. Stepped WC grain surfaces are arrowed in (b).

2.2.1 WC phase

WC has a simple hexagonal crystal structure (space group P6m2) with two atoms per unit cell and a *c/a* ratio of 0.976 (*a* = 0.2906 nm) [1]. W and C planes are alternately stacked along the direction [0001], see Figure 2.4a. The WC grains consist usually of a single crystal and are facetted with (0001) and {1-100} planes. The crystal structure is polar with two sets of three equivalent {10-10} planes, which gives the truncated triangular-prism shape to the crystals bounded by {1-100} faces [24], Figure 2.4b. The hardness on the (0001) planes is up to twice of that on other planes [25], and the cleavage strength is the lowest in the (0001) planes [26].

An example of a triangular shaped WC grain and its diffraction pattern is shown in Figure 2.5.
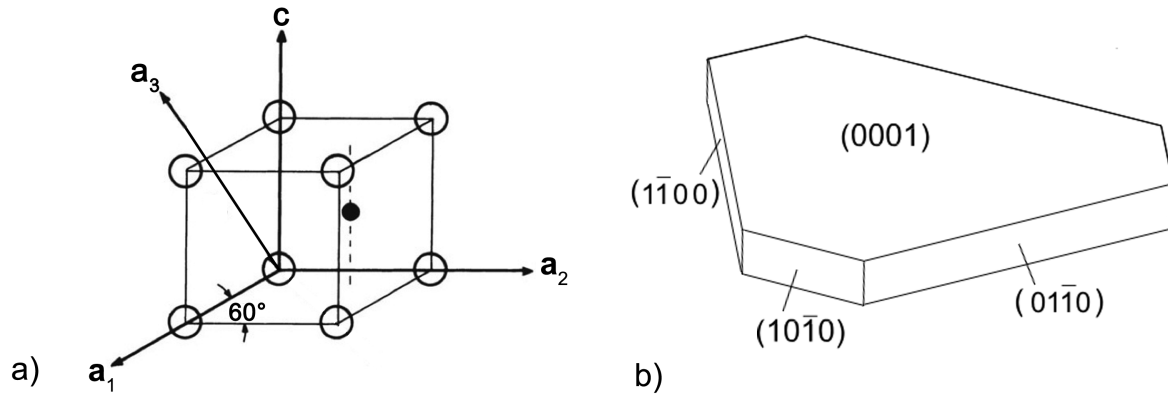

Figure 2.4: (a) The unit cell of WC with reference to the hexagonal axes $\mathbf{a}_1$, $\mathbf{a}_2$, $\mathbf{a}_3$, and $\mathbf{c}$. Open circles are tungsten atoms, and solid circles are carbon. (b) A schematic of the truncated triangular shape of a WC grain.

Much research has been carried out on WC grain growth during liquid-phase sintering of cemented carbides [2,27]. According to Lifshitz, Slyozov, and Wagner, the grain coarsening is limited by interfacial reactions or long-range diffusion. A coarsening process is predicted to obey a rate equation according to [28,29]:

$$r^n - r_0^n = 2Kt \qquad (2.5.1).$$

Where r is the average grain radius, r_0 is the initial average grain radius, K is a coarsening rate constant depending on the controlling mechanism, and t is the time. If the growth is controlled by an interface reaction, the exponent n will be 2. For the diffusion-controlled growth, n is equal to 3.

WC grain growth is known to be limited by the interface reaction rather than by diffusion [3]. The flat facetted surface of WC grains causes the atoms to attach normally to the surface. This requires a high energy to start the nucleation [30]. Surface defects are needed to reduce the energy barrier in order to nucleate an atom. Nucleation sites for grain growth may, however, be formed by dislocations emerging at the grain surface. The screw component of an emerging dislocation would provide a step defect on the grain surface.

In order to reduce the WC grain growth, grain growth inhibitors such as Cr or V are often added. These elements will segregate to WC/binder interfaces and WC/WC grain boundaries and make them stronger [31,32]. The Cr addition gives the WC grains sharp edges and stepped surfaces [33]. The solubility of different transition metals in the WC grains is very

low. J. Weidow et al. [34] studied the solubility of different transition metals in WC using atom probe tomography. The solubility of Ta, Nb, Cr, and V was in the range of 10^{-3} atom fraction; Ti and Mn had a lower solubility, while any solubility of Zr and Co could not be detected.
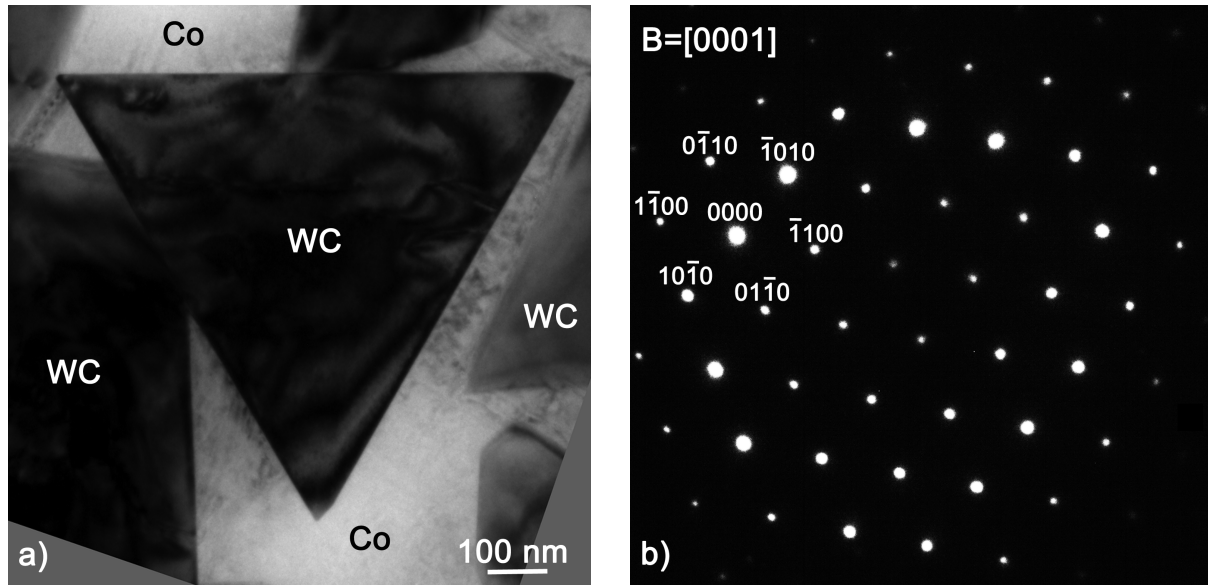

Figure 2.5: (a) A bright field TEM image of WC grains surrounded by a Co-rich binder phase. (b) The selected area electron diffraction pattern from the triangular WC grain in (a). This grain is oriented with its **c**-axis close to parallel to the incident electron beam.

2.2.2 Binder phase

Cobalt is the most commonly used binder for WC because of its excellent carbide wetting and adhesion properties. The capillary action of cobalt during sintering allows the achievement of high densities [35]. Other possible binders are Fe and Ni for example.

Cobalt exists in two allotropic forms, the hcp form which is stable at temperatures below 418 °C and the fcc form which is stable up to a temperature of 1495 °C, which is the melting point of pure cobalt [36]. However, a significant amount of fcc cobalt is present in sintered WC-Co hard metals at room temperature. The transformation between the two phases is martensitic in nature [37]. Co-rich binder phase contains significant amounts of W and C, and some of them remain in solid solution after cooling from sintering. The retention of the fcc structure to room temperature may be caused by the residual stress state imposed by the rigid WC skeleton, or by stabilization by solute elements.

8

2.2.3 Cubic carbides

It is possible to alloy WC-Co based cemented carbides in order to improve their properties and adapt them to different applications. Hard cubic carbides such as TiC, TaC and NbC are often added to the powder mixture during fabrication [38,39]. This will create new hard phases in addition to the WC phase. The TiC, NbC and TaC rich phases, harder than the WC phase, will consolidate the WC skeleton and make it harder (Figure 2.6).
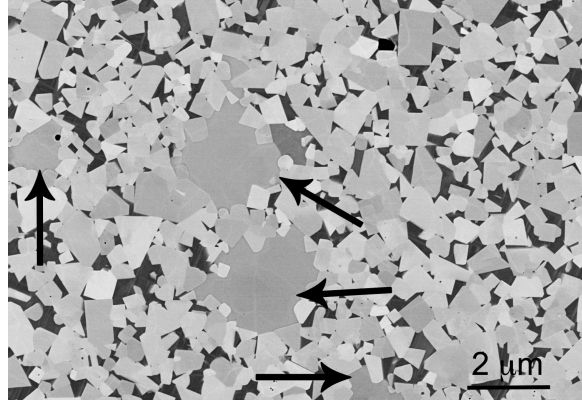

Figure 2.6: The microstructure of a WC-NbC-TaC-Co cemented carbide. Grains of cubic carbide are arrowed.

2.2.4 WC/Binder phase boundary

The boundary between WC and binder phase is the centre of big interest in WC grain growth investigations. Additions of grain growth inhibitors such as V or Cr resulted in the creation of V or Cr-rich thin cubic layer at the phase boundary [40]. These layers were observed by the mean of EDX in TEM first [41] then later with HRTEM [40,42,43]. Kawakami et al. [44] have investigated VC-doped WC-Co cemented carbides cooled down from sintering with different cooling rates. It was found that the V-rich layer was thinner for a rapidly cooled specimen.

2.2.5 WC/WC grain boundaries

WC grains form a strong and continuous skeleton for cemented carbides. However when these composite materials are used as tools they deform plastically and many of the grain boundaries are infiltrated by Co rich binder phase [45]. To overcome this problem and reinforce the grain boundaries, Ab initio calculations predicted that the segregation of Ti, V and Cr will lower the interface energy and increase the work of separation [31]. Co is also found to segregate to WC/WC grain boundaries in 0.5 − 1 monolayer [4,6,8]. The segregation

of Co is believed to also increase the work of separation and strengthen the grain boundaries [46,47]. Cr is predicted to segregate in 1 monolayer to the grain boundaries, and the strengthening effect of segregated Cr was less pronounced compared to Co.

2.3 Magnetic measurements

The metals used as binder phase in cemented carbides, like Co, Ni, and Fe are ferromagnetic. The magnetic induction B in the ferromagnetic material when placed in an external magnetizing field H is given by:

$$B = \mu_0 (H + M) \qquad (2.3)$$

where M is the magnetization of the material.

The coercivity, H_c, is the external field required to reduce the magnetization to zero after the material has been saturated. H_c is strongly influenced by the size of the of the ferromagnetic binder phase volumes; H_c is inversely proportional to the size of binder volumes. Larger magnetic domains in the Co-rich binder, i. e. large Co volumes, will result in a lower value of H_c. For a given volume fraction of binder phase, the dimensions of the binder volumes will depend on the WC grain size [17]. Larger WC grains will result in larger intergranular Co-rich volumes and a lower H_c. The coercivity may, thus, be used as a measure of the average WC grain size.

The magnetic saturation, M_s, is influenced by the binder phase composition. Dissolution of W reduces the value of M_s. When the C content of the binder is high, or if graphite has formed, the W content of the binder is low, and the M_s value increases.

These two magnetic properties are often used in industry for quality control. Coercivity is used to compare the size of WC grains of different materials after sintering, to detect whether there has been an unexpected grain growth or not. The magnetic saturation is used to estimate the C content in the binder phase in order to avoid creation of eta phase or graphite.

2.4 Mechanical properties

The mechanical properties of WC-Co cemented carbides at room temperature have been studied previously [48,49]. In the 1970's the industrial needs led to the characterization of these properties at elevated temperatures [11]. Like many other engineering materials, the mechanical properties of cemented carbides are strongly influenced by their microstructure, e. g. factors such as grain size and size distribution, binder phase volume fraction, and contiguity.

An example of the relation between microstructure and mechanical properties is the hardness of the material. Hardness is the measure of resistance to deformation. The carbide phase is primarily defining the hardness of the material, since it is very hard and the binder phase is soft and ductile. The volume fraction of the binder phase and the size of the WC grains are then important. A high hardness is achieved when the carbide volume fraction is high and the carbide grain size is small [50]. The fracture toughness generally shows an inverse relation to hardness. The determination of the microstructural parameters such as WC grain size and volume fraction will be explained in more detail in Chapter 3. The relationships between the mechanical properties and the mean WC grain size and the carbide volume fraction are known. The influence of WC grain shape and size distribution is, however, not yet clear, nor is the effect of the interface character distribution.

Sakuma et al. [51] have observed that the stress-strain (σ-ε) behaviour of cemented carbides is very sensitive to the WC grain size and the volume fraction of binder phase. The creep resistance increases with an increase of WC grain size at high temperatures, but the opposite holds at low temperatures. It was also observed that the flow stress is reduced with an increase of binder phase volume fraction.

2.5 Plastic deformation

Cemented carbide is a preferred material to use for metal cutting in the manufacturing industry. The very hard WC skeleton and the tough binder phase gives to the material the unique property of high resistance to deformation. However, cemented carbides still deform under certain conditions and the deformation mechanisms of the different phases vary.

The most observed plastic deformation mechanisms of cemented carbides are, plastic deformation of the binder phase [17], plastic deformation of WC grains by dislocation climb and glide [45], WC grain growth [51], accommodated WC/WC grain boundary sliding that results in WC grain boundary infiltration and binder lamella formation [9], unaccommodated WC/WC grain boundary sliding that results in cavity formation in the intergranular phase [17].

At low temperatures, cemented carbides are very brittle and deform elastically only. This is valid from room temperature up to 600 °C [13,14]. A couple of hundred degrees higher in temperature, deformation of the binder phase start to take place [52]. No plastic deformation of the WC has been observed at these temperatures, but some dislocations were present in the WC grains in the deformed material [53].

If a stress below the yield stress is applied, the material deforms elastically, i.e. the material is able to return to its original shape after the stress is removed. With larger stresses,

unrecoverable or plastic deformation occurs, i.e. the material yields. Crystalline phases will then deform along certain planes and directions, which are called slip systems.

During yield, the movement of dislocations takes place through a crystal lattice. Each time a dislocation moves through a crystal, part of the crystal moves one lattice point along a plane, relative to the rest of the crystal. The plane that separates both parts and along which the movement takes place is called a glide plane. To allow the movement, all atomic bonds along the plane have to be broken. If all bonds were broken at once, this would require very high energy. When the movement takes place step by step, the breaking of bonds is immediately followed by the creation of new ones and the energy required is much lower. Two types of dislocations exist; the simplest dislocation to visualize is called edge dislocation and it consists on inserting an extra half plane in a crystal while the second type consists of inserting a helical spiral defect in the crystal, this type is called screw dislocation. Dislocations may also be intermediate between edge and screw and are then called mixed dislocations [54].

During creep deformation the stress is below the macroscopic yield stress so dislocations cannot move directly by large scale glide. However, since the temperature is high diffusion occurs, and by diffusion an edge dislocation can move perpendicular to its glide plane, i.e. it can climb. By climb dislocations might pass over obstacles such as atoms dissolved in the lattice, small particles or other dislocations and then glide until stopped by the next obstacle. This so-called dislocation creep is expected to occur in the binder phase at sufficiently high temperature and load. As the binder phase deforms the WC skeleton will carry more and more of the load, and at certain locations such as contact points between WC grains the local stress in a WC grain might exceed the yield stress at the temperature in question. Then this grain deforms by dislocation glide, despite the fact that the macroscopic load is below the yield stress.

In work by Sakuma and Lee [55,56], WC grain growth under a compressive load was observed at high temperatures. In their case, abnormal WC grain growth was observed at temperatures higher than 1100 °C during deformation to high strains (30 – 120 %). In order to explain this abnormal grain growth Sakuma summarized a number of proposals for the reason for the WC grains to grow. Excess of vacancies generated near grain boundaries through grain boundary sliding was suggested by Clark and Alden [57]. Sato et al. suggested grain switching based on cellular dislocation climb [58]. The conclusion of this survey was that the proposed models couldn't be fully evaluated because of poor grain growth data.

Compressive creep deformation at 1200 °C resulted in a textured microstructure with the WC grains having a preferred orientation of [0001] normal to the load axis [51]. This might be caused by grain boundary sliding between WC grains. Grain boundary sliding at 1000 °C, and above, has also been observed in a number of other investigations [59–61]. Östberg et al.

observed binder infiltration in WC/WC grain boundaries and the formation of binder phase lamellae between adjacent WC grains [45]. The lamellae were generally oriented along the resultant load direction.

Cavity formation was observed in internal friction tests at temperatures above 1000 °C by D. Mari [17]. The cavities were formed in the binder phase and most of them in WC-binder-WC triple points. Adjacent to the cavities, deterioration of the WC/WC grain boundaries and WC/WC grain boundary sliding was often observed. The formation of cavities might be caused by diffusion of vacancies in the cobalt at the high temperature ($\geq$ 1100 °C).

Chapter 3 - Experimental techniques and procedures

3.1 Experimental materials

Two series of WC-Co based cemented carbides with different WC grain size were studied, see Table 3.1. The first series consisted of two WC-Co based cemented carbides with fine WC grain size (0.4 μm) destined for machining applications, an un-doped WC-Co material with 10 vol % binder phase, and a Cr-doped WC-Co material with a higher fraction of binder phase, 16 vol %. The starting WC powder to make the two materials of the first series had medium size, and the average diameter of the powder particles was 2 μm. The raw powders of WC and Co were milled for 60 hours to prepare the un-doped material, and for 50 hours with addition of Cr_3C_2 to prepare the Cr-doped material. Ball milling was carried out in a stainless steel container with addition of ethanol and wax.

The second series consisted of two WC-Co based cemented carbides with coarse WC grain size (1.4 μm) destined for mining applications, an un-doped, and a Cr-doped WC-Co materials. In both materials, the binder phase represents ~10 vol% of the total volume. To make the two materials of the second series, two different WC starting powders with different average WC particle sizes were used. A WC powder of FSSS value 5.6 μm was used in the starting powder mixture prepared for fabrication of the un-doped material. A WC powder with a FSSS value 6.25 μm was used in the fabrication of the Cr-doped material. The Co powder had an average particle size of 0.8 μm and the Cr_3C_2 powder had a FSSS size of 1.6 μm. Starting powder mixtures containing WC and Co or WC, Co and Cr_3C_2 and addition of 2 wt% Polyethylene glycol as pressing agent were ball milled in ethanol-10%H_2O in a stainless steel container for 11.5 hours.

The WC grain size and the composition of the binder phase are important parameters when a cemented carbide material is fabricated. Therefore, the coercivity and magnetic saturation of the different materials were determined after sintering, see Table 3.1. The two fine grained un-doped and Cr-doped materials were designed in a way they end up with the same WC grain size and had a coercivity of 25 and 19.9 kA/m, respectively. And their respective binder phase had a relative magnetic saturation (Co_m/Co) of 0.88 and 0.90, which puts the materials close to the graphite limit in the equilibrium phase diagram. The hardness of the un-doped

and Cr-doped fine-grained materials was 1840 and 1700 HV3, respectively. The second series with coarse-grained cemented carbides were also designed in a way both un-doped and Cr-doped materials will result with the same WC grain size after sintering. Both un-doped and Cr-doped materials had coarser WC grain size and a coercivity of 10.42 and 10.15 kA/m. The relative magnetic saturation of the binder phase in the un-doped and Cr-doped materials was 0.90 and 0.93.

Table 3.1. Composition and data of the materials investigated in this work.

Material		Composition [wt%] (balance W)			Binder Phase [vol%]	Mean Linear Intercept Length [μm]	Materials data		
		Co	Cr	C			H_c [kA/m]	$(Co)_m/Co$	HV3
Fine Grained Series	Un-doped	5.78	--	5.74	10	0.41	25	0.88	1840
	Cr-doped	8.37	0.84	5.58	16	0.41	19.9	0.90	1700
Coarse Grained Series	Un-doped	6.00	--	5.70	10	1.40	10.42	0.90	1393
	Cr-doped	6.00	0.60	5.73	10	1.40	10.15	0.93	1418

3.2 Hot compressive creep tests

3.2.1 Fabrication of test bars

Compressive creep specimens were prepared from the two series by Sandvik Coromant and Sandvik Mining and Construction. After spray drying the granules were pressed isostatically into cylindrical green bodies before being machined into the shape of a test bar. The shaped green bodies were later gas pressure sintered at 1410 °C with a holding time of one hour. The specimens were shaped before sintering in a controlled way so that the test bars ended up with the exact desired dimensions after sintering and final grinding of the grip. Once the test bars were sintered, the grip parts were ground and the gauge length remained unchanged. The final dimensions of the test bars were 42 mm in length, 12 mm in grip diameter, the smallest diameter was 6 mm, and the gauge length measured 12 mm, see Figure 3.1.

3.2.2 Compressive creep testing

In order to have controlled testing conditions, plastic deformation of the different materials from the two series was achieved in a hot compressive creep rig where a load of 900 MPa was applied at 900, 1000 and 1100 °C and 300 MPa at 1100 °C, and the test bars were deformed to different strains. The hot compressive creep test is close to the condition that the tool is

subjected to during machining. The choice of the applied load and the temperature was also close to the real machining conditions.
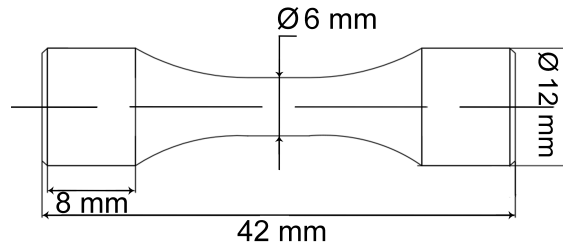

Figure 3.1: The geometry of the test bar.

The test bars from the fine-grained un-doped material were deformed at 900 and 1000 °C with an applied load of 900 MPa. The same load was applied to the fine-grained Cr-doped material at 900, 1000 and 1100 °C. The test bars from the coarse grained materials were deformed at 1000 °C under a load of 900 MPa and then at 1100 °C with a reduced applied load of 300 MPa. The load was reduced in order to stay in the intermediate steady state creep regime at 1100 °C. The new load was calculated from an equation that K. Buss has used in her work [62]. Where cemented carbides were creep tested with three point bending at temperature range 700 – 1200 °C. The activation energies were measured for the different creep mechanisms. The same creep mechanisms were found to be active at 1000 and 1100 °C, but the stress need to be reduced at higher temperature in order to keep the same strain rate during deformation.

The creep tests were carried out in a closed chamber under flowing argon in order to avoid decarburization or oxidation of the test bar. The test bar was surrounded by induction heating coils and the temperature was measured by a thermocouple. The change in gauge length was measured by an extensometer with a measuring range of 0 – 10 % strain. The test bar deformed to a total of 20 % strain was, therefore, deformed first to 10 % strain and then, after resetting the extensometer, to an additional 10 % strain. It is important that the heating coils were turned off at the end of the creep test, and that the temperature dropped very quickly.

The fine-grained Cr-doped material was also heat treated at 1000 °C in the same apparatus as the creep experiments were carried out. The heating and cooling was carried out exactly in the same way as the creep tests.

17

3.3 Quantitative microscopy

The quantitative microscopy carried out in this work consisted of extracting meaningful quantitative data from a scanning electron microscope (SEM). This includes both imaging and electron backscatter diffraction (EBSD) analysis. The work included the determination of the average WC grain size by the linear intercept method [63], the estimation of the binder phase fraction from binary images [64], and the determination of number density of infiltrated WC/WC grain boundaries. The average WC grain size was also estimated from data obtained by EBSD. This technique was, in addition, used for the assessment of binder phase grain size.

3.3.1 Linear intercept method

For each test bar, SEM images using backscattered electrons were obtained from two cross-sections: parallel and perpendicular to the load axis, see Figure 3.2. For each cross section, three different locations were investigated: at the centre, at the rim, and at half radius distance from the centre (Figure 3.2). The magnification of the SEM was set to 70000X for the fine-grained series and to 17000X for the coarse grained series.

Vertical and horizontal lines were drawn on the images, see Figure 3.3, and the length of a line intercepting a grain was measured. Mean linear intercepts perpendicular and parallel to the load axis were determined for both horizontal and vertical lines of the sections taken parallel to the axis. In the section taken perpendicular to the load axis, a mean linear intercept perpendicular to the load axis was determined [63]. An average WC grain size was then calculated at different distances from the centre of the test bar.
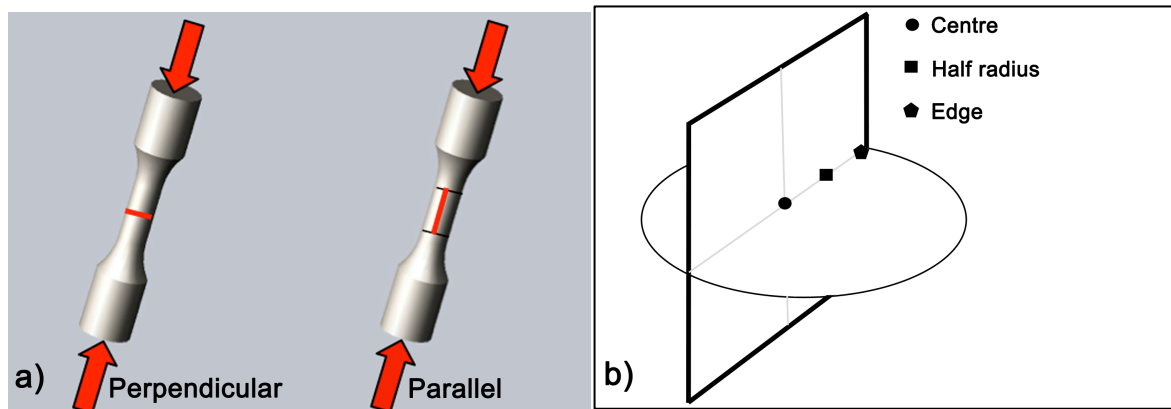

Figure 3.2: Parallel and perpendicular cross-sections of the test bar (a), and the different areas (centre, edge, and half radius distance) (b) investigated for each test bar.

A 95% confidential interval (CI) was determined for the average WC grain size from:

$$95 \% \; CI \; = t * s * n^{-1/2} \qquad (3.1)$$

Where s is the standard deviation of the measured intercept lengths and n is the number of measured intercepts [65]. The factor t is a multiplier related to the number of fields that were analysed. In this study t was equal to 2.571 (six fields) or 2.776 (five fields).
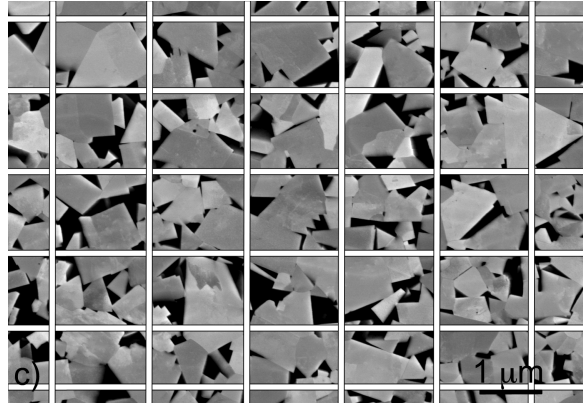

Figure 3.3: The linear intercept method.

3.3.2 Electron backscattered diffraction

The WC and binder phase grain sizes before and after deformation were assessed by EBSD analysis. The spread in local crystallographic orientation of the binder phase pockets was also investigated.

The analyses were performed in a LEO Ultra 55 FEG SEM equipped with a Nordlys EBSD camera and the HKL Channel 5 software. The acquisition of the EBSD data was carried out at an acceleration voltage of 20 kV and in high current mode using a 60 μm aperture. The specimen was tilted 70 ° towards the EBSD camera and the working distance was set to 13 mm. The camera was inserted as far as possible in order to get a large solid angle. The electron beam step size was set to 40 nm.

In the automated analysis of the acquired electron backscatter patterns (EBSP), the software looked for six to eight Kikuchi bands using the Hough transform. The results were compared with crystallographic parameters of 44 Bragg diffracting lattice planes (reflectors) in the relevant crystal structures. The Hough space transform was set at level 50. The post processing of the patterns was done with a noise reduction level of 4 and with wild spikes filtering.

The analysis of the EBSP results in the identification of phase and orientation, see Figure 3.4. Individual grain sections are identified by their different crystallographic orientations. The WC grain section area was determined by the software, and an equivalent circle diameter was calculated from the grain section area. The minimum grain section area in this evaluation was set to three pixels.

The internal strain in the WC grains, before and after creep deformation, was evaluated by the mean angular deviation (MAD), and the band contrast and band slope derived from the Hough transform. The MAD tells how well the simulated EBSP overlays the experimental EBSP, and gives, in degrees, the averaged angular misfit between the acquired and the simulated Kikuchi bands. The band contrast gives the average intensity of the Kikuchi bands compared to the total intensity within the EBSP expressed on a scale from 0 (low contrast) to 255 (high contrast). The higher the contrast, the better is the EBSP quality. The band slope shows the sharpness of the Kikuchi bands in the EBSP. It is also expressed on a scale of 0 to 255, and the higher the value, the sharper the Kikuchi band. A strained structure would reduce the EBSP quality, and thereby give a lower band contrast and a reduced band slope.

Orientation maps were used in order to detect any changes in the morphology and size of the binder phase grains during deformation. An orientation map describes the crystallographic orientation of the grains by using an Euler angle-based colour scale, see Figure 3.4b.
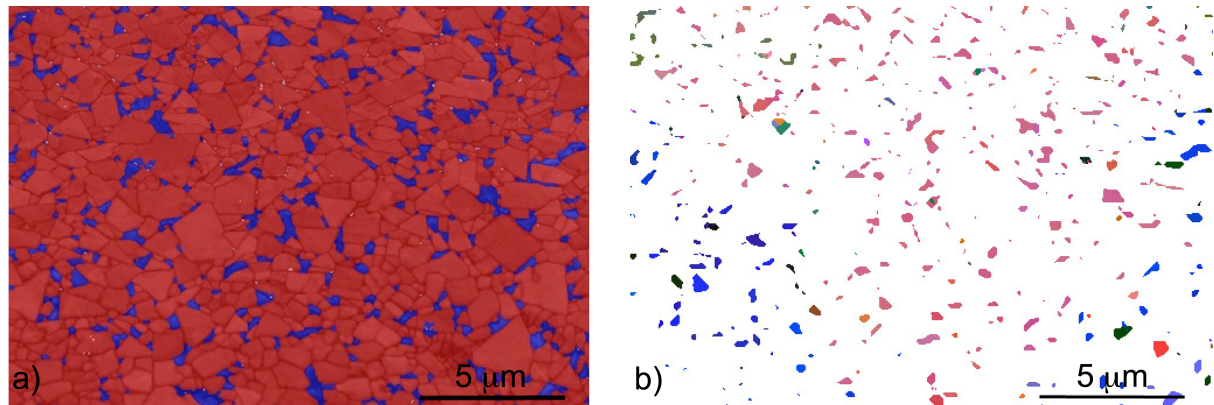

Figure 3.4: (a) An EBSD map showing the WC grains (red) and the Co-rich binder phase (blue). (b) An EBSD orientation map (All-Euler) of the Co-rich binder phase. (a) and (b) show the same area of Material 2 in the as-sintered condition.

3.3.3 Binary images

In order to estimate the intergranular volume fraction before and after creep deformation, the backscattered electron images taken from the cross sections perpendicular to the load axis

were converted to binary using the Digital Micrograph software, see Figure 3.5. The threshold level was adjusted so that the Co containing intergranular regions appeared with black contrast (0, zero intensity), and the WC grains with white contrast (255, full intensity). The average pixel value divided by 255 (full intensity) gave the area fraction of the WC grain sections, and the intergranular area fraction was the complement value to one.
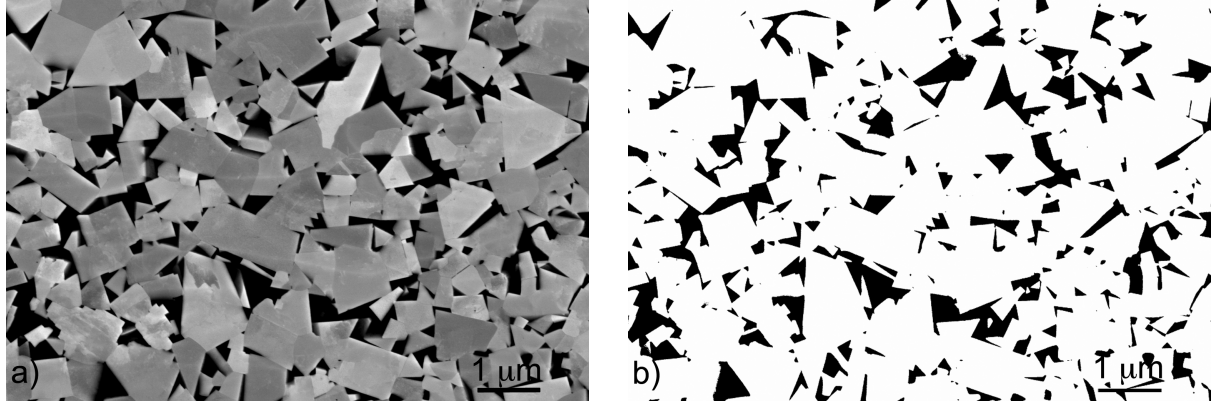

Figure 3.5: A backscattered electron image of the as-sintered Material 2 (a), and the corresponding binary image (b).

3.3.4 Number density of infiltrated WC/WC grain boundaries

The same backscattered electron images taken for the linear intercept measurements were also used to determine the number density of infiltrated WC/WC grain boundaries. That is to say, to determine the number of WC/WC grain boundaries containing a film of Co-rich binder phase per unit area.

3.4 Transmission electron microscopy

Transmission electron microscopy (TEM) allows for more detailed studies than SEM. The microstructure of the fine-grained Cr-doped material (Table 3.1) was investigated before and after creep deformation (20% at 1000 °C) in a FEI Tecnai T20 TEM. The instrument was operated at an acceleration voltage of 200 kV.

The microstructures were studied by bright and dark field imaging and selected area electron diffraction. A bright field image displays all phases in the microstructure, while a dark field image only shows areas with a specific crystallographic orientation. The distribution and crystallographic orientation of the Co-rich binder phase was investigated, see Figure 3.6. Special attention was paid to the WC grain shape and matrix dislocation density, see Figure 3.7.
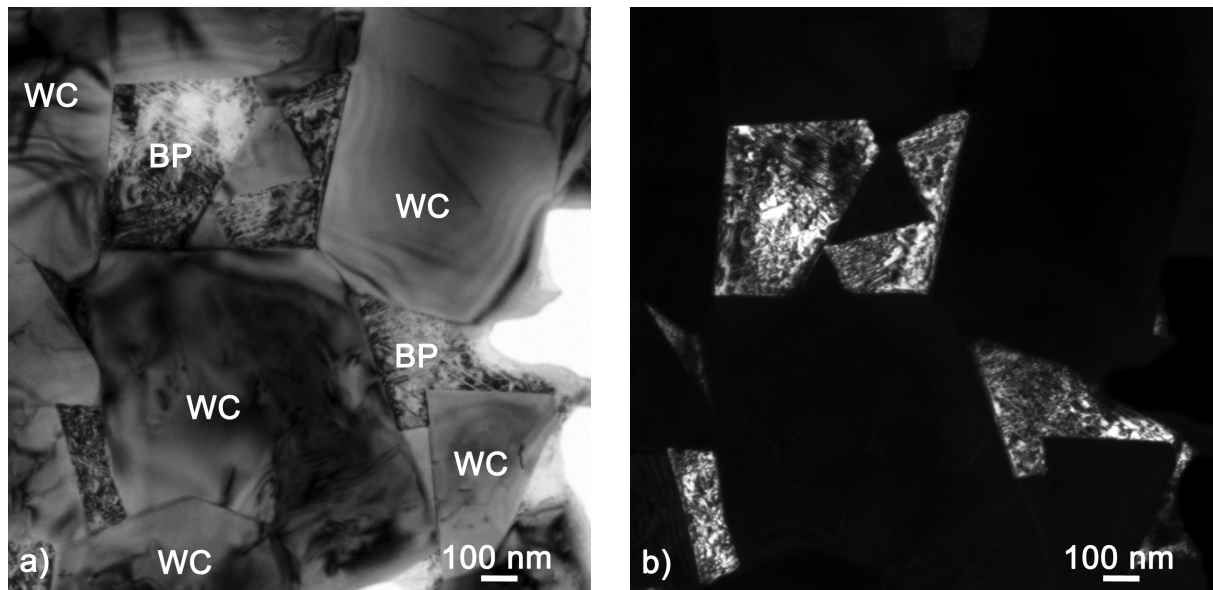
Figure 3.6: Bright field (a) and dark field (b) TEM images of a binder phase grain (BP) in Material 2 in the as-sintered condition.
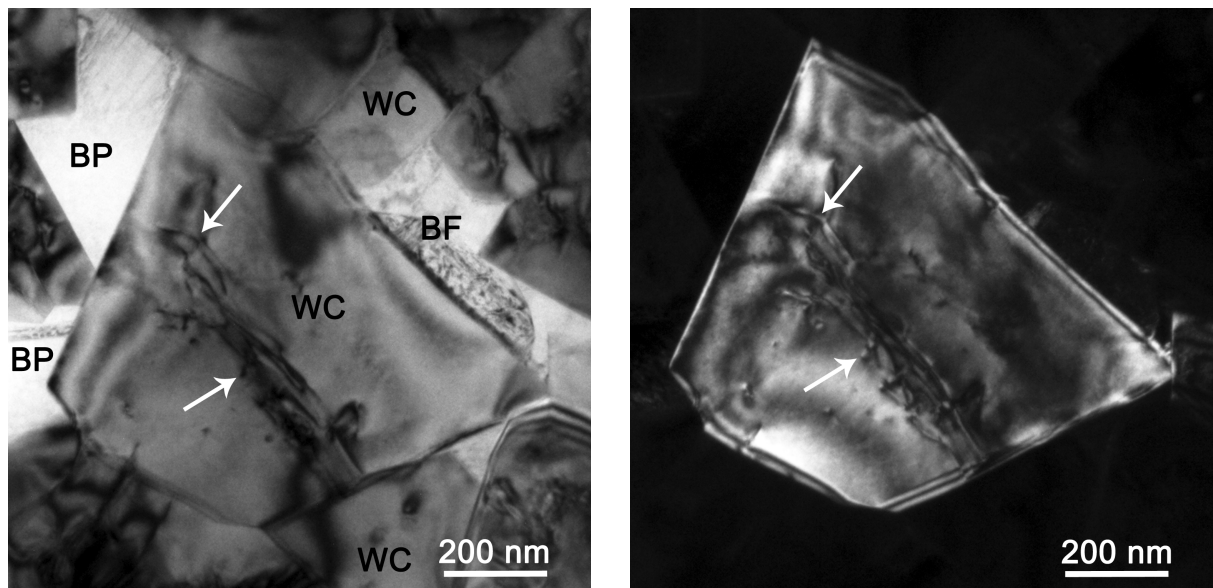

Figure 3.7: Bright field (a) and dark field (b) TEM images of a WC grain surrounded by binder phase pockets (BP) in Material 2 in the as-sintered condition. The dislocations are arrowed.

3.5 Atom probe tomography

The atom probe uses sharp specimen needles with a tip radius below 100 nm. Tips from the fine-grained un-doped and Cr-doped materials were analysed in an Imago LEAP 3000X HR

atom probe system. The specimen was placed in the analysis chamber facing a small aperture of 40 μm in diameter at ground potential, called the local electrode. The instrument was run with a specimen temperature of 66 K. Laser pulsing of the sample was carried out using a green light with a wavelength of 532 nm, a pulse frequency of 200 kHz, and a pulse energy of 0.34 nJ. Surface atoms at the tip of the specimen were field evaporated first. To avoid precocious fracture of the tip during analysis, the target evaporation rate was set to 0.2 % (detected ions per applied laser pulse) at the beginning of the analysis, and then increased to 1 % once the field evaporation became stable. The sharp needle was consumed along the analysis and the run was stopped when the tip is fractured. The experimental data analysis was done by the IVAS 3.6.10 software. An example of a 3D reconstruction of an analysed material is shown in Figure 3.8. Since two different phases were analysed and the binder phase has a lower evaporation field than WC, the transition from the binder phase to the WC grain will induce a sudden increase in the voltage. This increase in voltage will be interpreted by the software as an increase in the tip radius at the phase boundary [66].

Because the interest was to analyse the binder phase and the phase boundaries, the specimens had often a binder phase volume in the top of the tip. The shank angle method was used for reconstructing the tips, and obtain a reconstruction as close as possible to the shape of the real tip specimen. The method consists on determining the evolution of the tip radius, within a single phase, as function of the depth z and the shank angle α. The voltage evaporation was first used to reconstruct the starting phase and determine the initial tip radius and the shank angle, assuming the reconstructed volume having a conical shape. A final reconstruction of the tip specimen using the determined tip radius and the shank angle is then made. In this work, the investigation of the phase boundaries was achieved using the shank angle method after it does not show any distortion at the transition binder phase/WC. In the case where both WC and binder phase were present in the very top volume of the tip, a voltage method was used for the 3D reconstructions. In this case the evaporation field was set either to 38 or 61 $V(nm)^{-1}$ depending on whether the binder phase or the WC grain was analysed [5].

The peak decomposition method was used to correct the overlapping peaks in the mass to charge spectrum. The corrections were made automatically by the IVAS software, using the option peak decomposition. The specimen with small shank angle resulted in having a peak of Co^+ with a long tail covering some isotope peaks of Ni^+. This effect is assumed to be related to limited thermal conduction in the tip of the specimen. The corrections were done manually using the isotope abundance fractions.

For the investigation of a WC/Binder phase boundary, an isoconcentration surface (isosurface) can be constructed and delineates the investigated phase boundary within the reconstruction. A proxigram is then calculated across these isosurfaces. It consists of plotting the average of normal concentration profiles crossing the interface [67]. In this work, the

proxigram is the appropriate method to show a short range profile of mainly W, C, Co and Cr concentrations across a phase boundary and the ability to investigate segregation phenomena. The one sigma error levels, σ, for the concentration values are also calculated.
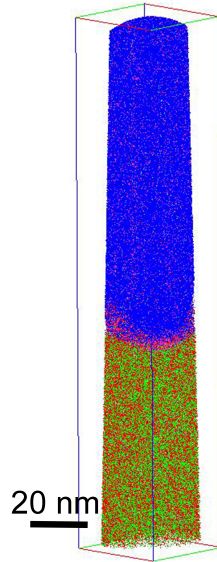

Figure 3.8: APT 3D reconstruction of the as-sintered fine-grained Cr-doped material.

3.6 Specimen preparation

3.6.1 Quantitative microscopy

EBSD is a surface analysis technique, since the diffraction pattern signal comes from a few nanometers from the surface. Thus the Kikuchi bands are sensitive to any damage of the crystal lattice within this layer. Therefore a good specimen preparation is really important. The surface of the specimen has to be mechanically polished to a mirror like finish free from scratches but this may introduce some residual strains at the surface. Ion polishing was used to remove the residual strains using the Gatan precision ion polishing system model 691 (PIPS).

The specimen should be small in order to fit in the holder of the PIPS, therefore thin slices of 250 μm thickness were cut from the gauge length of the compressive creep test bars. After polishing, the slices were cut to 5x5 mm pieces. Inside the chamber of the PIPS the upper surface of the specimen was sputtered by 4 keV Ar^+ ions at an angle of 2° during four hours.

The specimens prepared for EBSD were also imaged by backscattered electrons in the SEM.

3.6.2 Transmission electron microscopy

A slice of 250 μm was cut from the gauge length perpendicular to the load axis of the test bar. The slice was thinned down to 150 μm using a 15 μm grain size grinding disc. A disc of 3 mm diameter was cut from the thin slice using an ultrasonic disc cutter. After polishing the disc on both sides, it was dimple ground from both sides down to a thickness of 50 μm at the centre. When looking for dislocations in a TEM thin foil, it is important to take in consideration the deformation of the surface during dimple grinding, since the deformed layer can reach 20 μm under the surface. Therefore, for safety reasons, a thickness of 50 μm was left after dimple grinding.

To make the specimen electron transparent, the dimple ground disc was then ion milled using a Fischione (model 1010) ion mill. The specimen was sputtered with Ar^+ ions from both sides at an angle of 12° for six hours, and then continued with an angle of 10° until the built-in laser detected a hole through the specimen. The parameters of 4 kV voltage and 5 mA current were used.

3.6.3 Atom probe tomography

Electropolishing was used to prepare the very sharp needle-shaped specimens needed for APT. This procedure was done following these main steps. First, slices of 150 μm were cut from the gauge part of the compressive test specimen using a high-speed saw. Then, rods with square cross-sections were cut from the slices using a low-speed saw. One tip of the rod was repeatedly dipped in a highly viscous lacquer (Lacomite) until the tip was covered with a 2 mm layer of Lacomite. The electropolishing was performed at 29 V in an electrolyte consisting of 5% H_2SO_4 dissolved in ethanol that was cooled down to −30 °C. The rod was immersed in the prepared electrolyte surrounded by a ring made of gold used as a counter electrode. A cylindrical waist was formed selectively at the level of the counter electrode and the electropolishing continued until the waist no longer could support the weight of the lower part of the rod. After the fracture of the specimen at the level of the waist, two very sharp needles were obtained. A layer of oxide might be created during electropolishing, therefore a back-polishing step was required to remove the oxide layer and to target a specific region in the material. The back-polishing was performed in an electrolyte consisting of 5% H_2SO_4 dissolved in methanol and cooled this time to −20 °C. The electropolished tip and the counter electrode made of platinum were both dipped in the electrolyte, and short pulses of 20 V were given. To keep the tip as sharp as possible during back polishing, short pulses of 2×10 ms, 8×2 ms, 8×1 ms and 8×0.5 ms were applied.

A focused ion beam / scanning electron microscope (FIB/SEM; Fei DualBeam Versa 3D) was used to target a specific region in the materials. As its name indicates, the instrument consists

of an electron column used for imaging and an ion column for milling, separated by an angle of 52°. The milling is performed by sputtering the material with the high energy Ga^+ ions and the milling rate is determined by the ion beam current. During the preparation of APT specimens, a low voltage and current (10 kV, 300 pA) were used in order to decrease radiation damage due to sputtering.

Chapter 4 – Thermodynamic modelling

The research and development linking materials science and engineering with computer calculations and simulations in the last decade have given birth to a revolutionary approach for quantitative conceptual design of various materials [68]. With a comprehensive computational thermodynamics, composition and process parameters can be optimised and the lead-time for materials development reduced. For the production of cemented carbides, complex systems can be treated, which makes it possible to make calculations on commercial products, which often consist of more than 4 elements and several phases.

In general, software for computational thermodynamics uses Gibbs energy expressions that are stored in databases. Gibbs energy is chosen since it is minimized at equilibrium at constant temperature and pressure and those quantities are easy to control in experiments. Each phase is represented by an expression for Gibbs energy that is a function of composition, temperature and pressure. With a thermodynamic description of a system it is easy to calculate the influence that different elements have on the stability of e.g. different carbides. Determination of phase fractions and the solubility of elements in different carbides are also easily calculated. By such calculations it is possible to optimize composition and sintering temperature instead of using time consuming and expensive experiments in order to develop a new alloy.

As an example of an expression for the Gibbs energy, the model for the solid FCC binder phase used by Kaplan et al. in their assessment of the Co-Cr-C system [69] with the carbon occupying the octahedral interstitial sites results in the following expression for the molar Gibbs energy

$$G_m^{FCC} = \sum_M \sum_I y'_m y''_I \, {}^0G_{M:I}^{FCC} + RT\left(\sum_M y'_M \ln y'_M + \sum_I y''_I \ln y''_I\right) + {}^E G_m^{FCC} \qquad (1)$$

where, *M* denotes metallic elements (Co and Cr), *I* denotes interstitial (C and vacancies) components and y'_M and y''_I are the site fractions of component M and I on sublattice 1 and 2,

respectively. $^0G_{M:Va}^{FCC}$ is the molar Gibbs energy of the pure element in the solid FCC binder, and $^0G_{M:C}^{FCC}$ is the molar Gibbs energy of the hypothetical carbides CoC and CrC. The second term represents the entropy of mixing and the last term represents the molar excess Gibbs energy and (disregarding the magnetic interaction) is described as

$$^EG_m^{FCC} = y'_{Co}y'_{Cr}\sum_I y''_I L_{Co,Cr:I}^{FCC} + y''_C y''_{Va}\sum_M y'_M L_{M:C,Va}^{FCC} \qquad (2)$$

In the assessment of the system, the values (as a function of temperature) of the four $^0G_{M:I}^{FCC}$ energies as well of the parameters $L_{Co,Cr:C}^{FCC}$, $L_{Co,Cr:Va}^{FCC}$, $L_{Co:C,Va}^{FCC}$, $L_{Cr:C,Va}^{FCC}$ are the quantities that need to be determined. The quality of the predictions from calculations is dependent on the quality of the thermodynamic database that is used. The thermodynamic data is frequently extrapolated from binary and ternary systems. The assessments are based on the available experimental information at the time and compromises are often made in order to describe the whole composition range without taking into account that certain parts are more relevant than others and thus demands a higher accuracy [70]. Such critical evaluations together with new experimental information should be, and has been, the basis when developing a thermodynamic database specialized for cemented carbides.

Chapter 5 – Results and discussion

5.1 Summary of appended papers

5.1.1 Paper I: Evolution of the microstructure during creep testing of WC-Co based cemented carbide

The evolution of the microstructure of a Cr-doped WC-Co based cemented carbide during high temperature creep deformation was investigated. Special attention was given to the determination of WC grain size and binder phase lamella formation. A compressive creep test was performed at 1000 °C under an applied load of 900 MPa for 700 seconds. Both linear intercept method and EBSD were used to determine WC grain size before and after creep deformation. In a cross-section perpendicular to the load axis, the EBSD analysis as well as the linear intercept method indicated a coarsening of the WC grains. Grain growth was also indicated by the EBSD analysis of a cross-section parallel to the load axis. The linear intercept method showed, on the other hand, a virtually unchanged average grain size on the section parallel to the load axis. The combined results indicate, hence, that WC grain growth took place during compressive creep deformation at 1000 °C. Furthermore, the linear intercept measurements suggest that this grain growth takes place preferentially perpendicular to the load axis. One explanation for WC grain growth at this relatively low temperature would be that plastic deformation of the WC grains leads to dislocations emerging at the grain surfaces. The dislocations with a screw component would facilitate the nucleation of atomic layers of W and C, and thus contribute to grain growth. The increased number of un-indexed pixels in the EBSD maps of specimens taken from the crept tested bar is a sign of plastically deformed WC grains. In addition, formation of binder phase lamellae at some WC / WC grain boundaries was observed after creep deformation. This would be caused by the movement of WC grains inside the binder phase matrix. Shear stresses created in WC / WC grain boundaries would result in grain separation at grain boundaries lying along a local load axis, and this may be followed by the infiltration of Co. It is, hence, suggested that also grain boundary sliding contributes to the deformation of the material.

5.1.2   Paper II: Deformation mechanisms in a WC-Co based cemented carbide during creep

In order to understand the mechanisms behind creep deformation of cemented carbide materials, the microstructure of a WC-Co based cemented carbide has been investigated before and after plastic deformation at high temperatures. The material was Cr-doped with fine WC grain size. Hot compressive creep tests were performed under an applied load of 900 MPa at 1000 and 1100 °C. From quantitative microscopy, the crept materials showed that WC grain growth took place during deformation, and that the growth took place preferentially in the plane perpendicular to the load axis. It is known that the WC grain growth is limited by interface reaction rather than by diffusion. It is suggested that matrix dislocations emerging at the WC grain surface may act as nucleation sites for growth of new layers of WC. A clear increase in the dislocation density in the WC grains after deformation was observed in the TEM. The EBSD analyses of the WC grains showed an increase in the MAD value and a decrease in the band contrast and band slope values after deformation. These observations suggest that the WC grains in the crept specimens had a strained structure. The redistribution of WC grains during creep resulted in the formation of binder phase lamellae. This suggests that grain boundary sliding contributes to the deformation of the material during creep testing. Intergranular cavity formation was observed in the SEM images of the crept materials. This indicates that also unaccommodated grain boundary sliding took place during deformation. EBSD analysis showed that the binder phase grains became smaller after deformation and lost their dendritic morphology. This was shown by an increase spread in the crystallographic orientation, which may be explained by binder phase grain rotation induced by dislocation glide.

5.1.3   Paper III: The creep behaviour of un-doped and Cr-doped WC-Co cemented carbide materials

Coarse-grained un-doped and Cr-doped WC-Co based cemented carbide materials have been investigated before and after plastic deformation at high temperatures. Hot compressive creep tests were performed under an applied load of 900 MPa at 1000 °C and 300 MPa at 1100 °C. The Cr-doped material showed better creep resistance. The two materials showed similar deformation mechanisms but the deformation occurred within different time scales. WC grain growth occurred during creep deformation in the plane perpendicular to the load axis. It took longer time for the Cr-doped material to reach the same WC grain size. This suggests that WC grain growth perpendicular to the load axis would be rate limiting in the creep deformation process. Some WC/WC grain boundaries of the two materials were infiltrated by the Co-rich binder phase, which suggests that accommodated grain boundary sliding also occurred. Some of the infiltrated grain boundaries had a step surface following a crystallographic orientation.

Cavity formation was also observed in the two materials. This suggests that unaccommodated grain boundary sliding also contribute to the deformation of the materials.

5.1.4   Paper IV: Atom probe analysis of the binder phase and phase boundaries in undoped and Cr-doped WC-Co cemented carbides

The effect of creep deformation and heat-treatment on the composition of the binder phase and the phase boundary segregation was investigated by the mean of atom probe tomography. An un-doped material was crept at 900 and 1000 °C and a Cr-doped material was crept at 900, 1000 and 1100 °C. The Cr-doped material was also heat-treated at 1000 °C. The test bars were cooled down very quickly from the test temperature in order to freeze in the composition at the test temperature, while the as-sintered materials were cooled down very slowly after sintering. In the as-sintered condition of the Cr-doped material, segregation of Cr to the WC/binder phase boundary was observed and a thin layer of 6 monolayers in thickness of (Cr,W)C was found to form on the surface of a WC grain facing the binder phase. This last layer was not found in the material heat-treated at 1000 °C, but the Cr segregation at the phase boundary was present. The thermodynamic calculations found that the (Cr,W)C phase is stable below 940 °C when no M_7C_3 carbides are formed in the material. The concentration of W and C in the binder phase of the Cr-doped material increased with increasing temperature, due to some WC grains that dissolved at elevated temperature. Because the crept test bars stayed at high temperature only for a short time, this was not enough to reach the equilibrium at the test temperature. The heat-treated material had after a long period of time at 1000 °C a binder phase composition close to the one predicted by thermodynamic calculations.

5.1.5   Paper V: The effect of WC grain size on the creep behaviour of WC-Co cemented carbides

The effect of WC grain size on the creep behaviour of WC-Co cemented carbides. Two undoped materials were investigated, a fine-grained and a coarse-grained cemented carbide. The two materials were designed in a way they end up with the same volume fraction of binder phase, the same magnetic saturation and were sintered in the same way. Compressive creep test were achieved at 1000 °C under a load of 900 MPa to a strain close to 10 % for both materials. The coarse-grained material showed better creep resistance but bigger cavities were formed in the material. Both materials showed a sign of grain boundary sliding and many WC/WC grain boundaries were infiltrated by the binder phase. The fine-grained material showed infiltration in a shape of saw-tooth like and lamella, while the coarse-grained material only showed saw-tooth like WC surfaces facing the infiltrated films. This was explained by the surface energy of the infiltrated WC surfaces that rearrange the atoms at the surface to

form step surfaces in order to minimize its surface energy. The fine-grained material having more phase boundaries will form more low energy surfaces during sintering.

5.2   Discussion

When WC-Co cemented carbides are used in tooling applications they are exposed to very high stresses and temperatures leading to the plastic deformation of the substrate and failure of the tool. The work done in this thesis is to determine the activated deformation mechanisms and to understand the behaviour of the material during such severe conditions. The choice of performing high temperature compressive creep tests was to deform the materials under controlled conditions i.e. temperature and stress. WC grain growth perpendicular to the load axis was found to occur during creep deformation at 1000 and 1100 °C. In paper 1 the focus was put in the determination of the average WC grain size by the mean of linear intercept method (LIM) and EBSD. LIM was selected for the grain size determination after it showed the preferential grain growth perpendicular to the load axis. The EBSD failed in showing the preferential grain growth after it considers the WC grains circular. WC grain growth is known to be limited by interface reaction rather than by diffusion, and the slow interface reaction is believed to be caused by slow nucleation of successive atomic layers onto WC surfaces. Dislocations with screw component emerging at the grain surface would create step defects on the grain surface and act as a nucleation point for grain growth. Already in the EBSD patterns created in paper 1, it was possible to see signs of plastic strain in WC grains. In paper 2, the TEM investigation showed clearly a significant increase in the dislocation density inside the WC grains, which is a sign of plastic deformation of WC grains during creep. Also the investigation of a heat treated material at the same temperature as the crept materials did not show any grain growth since no strain was created in the material. Paper 3 linked the grain growth to the strain by comparing the same material deformed to different strains and temperatures. It was found that the grain growth is associated with strain and not temperature or time, which agrees with the proposition that WC grain growth is limited by the interface reaction rather by diffusion. The comparison of un-doped and Cr-doped materials in paper 3 showed a higher creep resistance of the Cr-doped material, the two materials deformed in the same way but it took longer time for the Cr-doped material to reach the same strain as the un-doped material. The Cr is added as a grain growth inhibitor, and segregates to the phase boundary. The Cr atoms at the surface of WC grains need to be replaced by W and C atoms in order for the WC grains to grow. This process of replacing the Cr atoms requires time, and thus slows down grain growth. This suggests that WC grain growth is rate limiting in the creep deformation process.

Another deformation mechanism found in this work was WC/WC grain boundary sliding followed by the Co-rich binder phase infiltrating the grain boundaries. In paper 1,2 and 3, an increased number of grain boundaries containing a film of the Co-rich binder phase was

observed in all the investigated materials crept at 1000 and 1100 °C. The applied compressive stress will introduce a shear stress and local tensile stress in WC/WC grain boundaries. This will push adjacent WC grains apart and may be accommodated by the infiltration of the Co-rich binder into the grain boundary. The infiltrated grain boundaries had two different morphologies; some had a lamella shape and others a saw-tooth like shape. When the Co-rich binder infiltrates a grain boundary, it forms a film between the adjacent WC grains. If the surface energy of the infiltrated grain boundary is low the film will have a shape of a lamella, otherwise dissolution and reprecipitation process will take place to reduce the surface energy and a stepped interface is formed. In paper 5 more stepped interfaces were observed in the coarse-grained material while lamella shaped films were found in the fine-grained material and the stepped interfaces were fewer.

Unaccommodated grain boundary sliding also occurred during the creep deformation and resulted in the formation of cavities. The infiltration of grain boundaries requires sufficient Co mobility and also neighbouring supply of Co. By the mean of EBSD, Co was found to redistribute during creep and the large finger-like Co grains divided into small grains (paper 2). Larger number and size of cavities were observed in coarse-grained materials compared to materials with fine WC grain size. The WC grain size can affect the redistribution of the binder phase causing creation of cavities (paper 5).

The APT investigation in paper 4 of the as-sintered Cr-doped material showed segregation of Cr to the WC/binder phase boundary of 0.8 monolayer and a thin layer of $(Cr,W)C$ of 6 monolayers was found to form on the surface of WC grains facing the binder phase. The material heat-treated at 1000 °C also showed segregation of 0.36 monolayer of Cr to the phase boundary but no $(Cr,W)C$ layer was found. The thermodynamic calculations predicts this layer to form below 940 °C when no M_7C_3 phase is formed in the material. The composition of the binder phase in the crept materials did not match the predicted composition from thermodynamic calculations. Transport of W and C in the binder phase during creep due to grain growth creates gradients and variation in the composition.

Chapter 6. Conclusions and outlook

- Preferential WC grain growth takes place in the plane perpendicular to the load axis during compressive creep testing at 1000 and 1100 °C.

- The preferential WC grain growth is rate limiting during creep deformation at 1000 and 1100 °C.

- The addition of Cr slows down the WC grain growth, and, as a consequence improves the creep resistance.

- Cr segregates in the Co-rich binder phase to the WC/binder phase boundary and this segregation is stable at 1000 °C.

- A thin layer of cubic (Cr,W)C also forms on WC grain surfaces in contact with the binder phase during cooling from the sintering temperature. This layer is believed to form below 940 °C.

- WC grain boundary sliding, accommodated by the infiltration of the Co-rich binder phase in WC/WC grain boundaries, occurs during creep testing at 1000 and 1100 °C.

- Unaccommodated WC grain boundary sliding also occurs during creep testing resulting in the formation of intergranular cavities.

The results from this work suggest that the following topics should be studied further:

- APT to determine the binder phase composition of heat-treated materials at 900, 1000 and 1100 °C followed by fast cooling.

- The crystallographic orientation of WC grain surfaces that form (Cr,W) carbide layer.

- The composition of binder phase films that infiltrates WC/WC grain boundaries.

- The crystallographic orientation of WC grains that are infiltrated by the binder phase.

- TEM investigation of abnormal WC grains.

- HRTEM of dislocations emerging on WC grain surfaces.

Acknowledgements

References

[1]   H. E. Exner, *Physical and chemical nature of cemented carbides*, *Int. Met. Rev.* **24** (1979) 149–173.

[2]   K. Mannesson, I. Borgh, A. Borgenstam, and J. Ågren, *Abnormal grain growth in cemented carbides—Experiments and simulations*, *Int. J. Refract. Met. Hard Mater.* **29** (2011) 488–494.

[3]   K. Mannesson, J. Jeppsson, A. Borgenstam, and J. Ågren, *Carbide grain growth in cemented carbides*, *Acta Mater.* **59** (2011) 1912–1923.

[4]   J. Weidow and H.-O. Andrén, *Grain and phase boundary segregation in WC–Co with small V, Cr or Mn additions*, *Acta Mater.* **58** (2010) 3888–3894.

[5]   J. Weidow and H.-O. Andrén, *APT analysis of WC–Co based cemented carbides*, *Ultramicroscopy.* **111** (2011) 595–599.

[6]   A. Henjered, M. Hellsing, H.-O. Andrén, and H. Nordén, *Quantitative microanalysis of carbide/carbide interfaces in WC–Co-base cemented carbides*, *Mater. Sci. Technol.* **2** (1986) 847–855.

[7]   H.-O. Andrén, U. Rolander, and P. Lindahl, *Phase composition in cemented carbides and cermets*, *Int. J. Refract. Met. Hard Mater.* **12** (1994) 107–113.

[8]   J. Gurland and J. T. Norton, *Role of the binder phase in cemented tungsten carbide-cobalt alloys*, *Trans. AIME.* **194** (1952) 1051–1056.

[9]   G. Östberg and H.-O. Andrén, *Microstructural changes during wear by plastic deformation of cemented carbide and cermet cutting inserts*, *Metall. Mater. Trans. A.* **37** (2006) 1495–1506.

[10]   S. Lay and J.-M. Missiaen, Microstructure and morphology of hardmetals. V. K. Sarin, D. Mari, L. Llanes, C. E. Nebel. **1** (2014) 91-120.

[11]   J. T. Smith and J. D. Wood, *Elevated temperature compressive creep behaviour of tungsten carbide-cobalt alloys*, *Acta Metall.* **16** (1968) 1219.

[12]   M. J. Murray and D. C. Smith, *Stress induced cavitation in cobalt bonded tungsten carbide*, *J. Mater. Sci.* **8** (1973) 1706–1710.

[13]   H. Suzuki, K. Hayashi, Y. Taniguchi, and H. Matsubara, *The Bend Deformation of WC–Co Cemented Carbides at Temperatures up to 1273 K*, *Trans. Japan Inst. Met.* **23** (1982) 77–84.

[14] H. S. Mohand, G. Fantozzi, G. Orange, and J. Dubois, *Comportement mécanique à haute temperature des carbures cementes WC–Co*, Rev Int Hautes Tempér Refract. **19** (1982) 311–323.

[15] H. M. Ortner, P. Ettmayer, and H. Kolaska, *The history of the technological progress of hardmetals*, Int. J. Refract. Met. Hard Mater. **44** (2014) 148–159.

[16] B. Roebuck and E. A. Almond, *Deformation and fracture processes and the physical metallurgy of WC–Co hardmetals*, Int. Mater. Rev. **33** (1988) 90–112.

[17] D. Mari, *Déformation à haute temperature des composites WC-Co*, PhD thesis, Ecole Polytechnique Fédérale de Lausanne, 1991.

[18] G. S. Upadhyaya, *Cemented tungsten carbides: production, properties and testing*, Noyes publications, 1988.

[19] J. Weidow, *Effect of metal and cubic carbide additions on interface chemistry, phase composition and grain growth in WC-Co based cemented carbides*, PhD thesis, Chalmers University of Technology, 2010.

[20] R. Porat, S. Berger, and R. Rosen, *Investigation of the sintering mechanisms for cemented carbides based on nanocrystalline powders*, Eur. Conf. Adv. Hard Mater. Prod. (1996) 101–107.

[21] H.-O. Andrén, *Microstructures of cemented carbides*, Mater. Des. **22** (2001) 491–498.

[22] C. H. Allibert, *Sintering features of cemented carbides WC–Co processed from fine powders*, Int. J. Refract. Met. Hard Mater. **19** (2001) 53–61.

[23] W. D. Kingery, H. K. Bowen, and D. R. Uhlmann, *Introduction to ceramics, Jhon Willey Sons, New York, 1976.*

[24] D. N. French and D. A. Thomas, *Crystallographic polarity of WC*, , in *Anisotropy in Single-Crystal Refractory Compounds*, (1968) 55–66.

[25] T. Takahashi and E. J. Freise, *Determination of the slip systems in single crystals of tungsten monocarbide*, Philos. Mag. **12** (1965) 1–8.

[26] S. Bartolucci Luyckx and J. Katzourakis, *Preparation and properties of WC–Co textured components*, Mater. Sci. Technol. **7** (1991) 472–474.

[27] R. M. German, *The contiguity of liquid phase sintered microstructures*, Metall. Trans. A. **16** (1985) 1247–1252.

[28] I. M. Lifshitz and V. V Slyozov, *The kinetics of precipitation from supersaturated solid solutions*, J. Phys. Chem. Solids. **19** (1961) 35–50.

[29] C. Wagner, *Theory of precipitate change by redissolution*, Z. Elektrochem. **65** (1961) 581–591.

[30] W. K. Burton and N. Cabrera, *Crystal growth and surface structure. Part I*, Discuss. Faraday Soc. **5** (1949) 33–39.

[31] M. Christensen and G. Wahnström, *Strength and reinforcement of interfaces in cemented carbides*, Int. J. Refract. Met. Hard Mater. **24** (2006) 80–88.

[32] J. Weidow, S. Norgren, and H.-O. Andrén, *Effect of V, Cr and Mn additions on the microstructure of WC–Co*, Int. J. Refract. Met. Hard Mater. **27** (2009) 817–822.

[33] M. Christensen, G. Wahnström, C. Allibert, and S. Lay, *Quantitative analysis of WC grain shape in sintered WC-Co cemented carbides*, *Phys. Rev. Lett.* **94** (2005) 66105.

[34] J. Weidow, S. Johansson, H. -O. Andrén, and G. Wahnström, *Transition metal solubilities in WC in cemented carbide materials*, *J. Am. Ceram. Soc.* **94** (2011) 605–610.

[35] A. A. Ogwu and T. J. Davies, *Proposed selection rules for suitable binders in cemented hard metals with possible applications for improving ductility in intermetallics*, *J. Mater. Sci.* **27** (1992) 5382–5388.

[36] H. Winterhager and J. Kruger, *Pure cobalt and its properties*, *Cobalt.* **29** (1965) 185–195.

[37] G. Wirmark and G. L. Dunlop, *Phase transformations in the binder phase of Co-WC cemented carbides*, *Sci. hard Mater.* pp. 311–328, 1983.

[38] J. Weidow and H.-O. Andrén, *Grain and phase boundary segregation in WC–Co with TiC, ZrC, NbC or TaC additions*, *Int. J. Refract. Met. Hard Mater.* **29** (2011) 38–43.

[39] J. Weidow, J. Zackrisson, B. Jansson, and H.-O. Andrén, *Characterisation of WC-Co with cubic carbide additions*, *Int. J. Refract. Met. Hard Mater.* **27** (2009) 244–248.

[40] A. Delanoë, M. Bacia, E. Pauty, S. Lay, and C. H. Allibert, *Cr-rich layer at the WC/Co interface in Cr-doped WC–Co cermets: segregation or metastable carbide?*, *J. Cryst. Growth.* **270** (2004) 219–227.

[41] A. Egami, M. Ehira, and M. Machida, *Morphology of vanadium carbide in submicron hardmetals*, *Kobe Res. Dev.* **44** (1994) 63–66.

[42] T. Yamamoto, Y. Ikuhara, and T. Sakuma, *High resolution transmission electron microscopy study in VC-doped WC–Co compound*, *Sci. Technol. Adv. Mater.* **1** (2000) 97–104.

[43] T. Yamamoto, Y. Ikuhara, T. Watanabe, T. Sakuma, Y. Taniuchi, K. Okada, and T. Tanase, *High resolution microscopy study in Cr3C2-doped WC-Co*, *J. Mater. Sci.* **36** (2001) 3885–3890.

[44] M. Kawakami, O. Terada, and K. Hayashi, *Effect of sintering cooling rate on V segregation amount at WC/Co interface in VC-doped WC-Co fine-grained hardmetal*, **51** (2004) 576–585.

[45] G. Östberg, K. Buss, M. Christensen, S. Norgren, H.-O. Andrén, D. Mari, G. Wahnström, and I. Reineck, *Mechanisms of plastic deformation of WC–Co and Ti (C, N)–WC–Co*, *Int. J. Refract. Met. Hard Mater.* **24** (2006) 135–144.

[46] M. Christensen and G. Wahnström, *Effects of cobalt intergranular segregation on interface energetics in WC–Co*, *Acta Mater.* **52** (2004) 2199–2207.

[47] M. V. G. Petisme, S. A. E. Johansson, and G. Wahnström, *A computational study of interfaces in WC–Co cemented carbides*, *Model. Simul. Mater. Sci. Eng.* **23** (2015) 45001.

[48] L. S. Sigl and H. F. Fischmeister, *On the fracture toughness of cemented carbides*, *Acta Metall.* **36** (1988) 887–897.

[49] N. Ingelstrom and H. Nordberg, *The fracture toughness of cemented tungsten carbides*, *Eng. Fract. Mech.* **6** (1974) 597–607.

[50] G. E. Dieter, *Elements of the theory of plasticity*, *Mech. Metall.* pp. 76–79, 1988.

[51] T. Sakuma, *High-Temperature Plastic Flow in Cemented Carbides and Cermets*, *Key Eng. Mater.* **108** (1995) 435–448.

[52] Y. V Milman, S. Luyckx, V. A. Goncharuck, and J. T. Northrop, *Results from bending tests on submicron and micron WC–Co grades at elevated temperatures*, *Int. J. Refract. Met. Hard Mater.* **20** (2002) 71–79.

[53] K. Buss and D. Mari, *High temperature deformation mechanisms in cemented carbides and cermets studied by mechanical spectroscopy*, *Mater. Sci. Eng. A.* **370** (2004) 163–167.

[54] I. Kovács and L. Zsoldos, *Dislocations and Plastic Deformation: International Series of Monographs in Natural Philosophy*. **60** (2013) 60.

[55] T. Sakuma and H. Hondo, *Plastic flow in WC-13wt.%Co at high temperatures*, *Mater. Sci. Eng.* 125–130, 1992.

[56] I. C. Lee, H. Hondo, and T. Sakuma, *Nonuniform carbide grain growth during high-temperature compressive deformation in WC-13wt% Co*, *Scr. Metall. Mater.* **28** (1993) 97–102.

[57] M. A. Clark and T. H. Alden, *Deformation enhanced grain growth in a superplastic Sn-1% Bi alloy*, *Acta Metall.* **21** (1973) 1195–1206.

[58] E. Sato, K. Kuribayashi, and R. Horiuchi, *A Model of Grain Growth Induced by Superplastic Deformation Based on Grain Switching*, *J. Japan Inst. Met.* **55** (1991) 839–847.

[59] J. G. Baldoni and W. S. Williams, *Deformation of cemented carbides*, *Am. Ceram. Soc. Bull.* **57**, 1978.

[60] S. Lay, J. Vicens, and F. Osterstock, *High temperature creep of WC-Co alloys*, *J. Mater. Sci.* **22** (1987) 1310–1322.

[61] R. J. Gottschall, W. S. Williams, and I. D. Ward, *Microstructural study of hot-deformed cemented carbides*, *Philos. Mag. A.* **41** (1980) 1–7.

[62] K. Buss, *High Temperature Deformation Mechanisms of Cemented Carbides and Cermets, PhD thesis, Ecole Polytechnique Fédérale de Lausanne*, 2004.

[63] International Organization For Standardization, *ISO 4499-2:2008, Hardmetals - Metallographic determination of microstructure. Part 2: Measurement of WC grain size, International Standards Organization*, pp. 1–17, 2008.

[64] W. T. Young, L. K. L. Falk, H. Lemercier, V. Peltier-Baron, Y. Menke, and S. Hampshire, *The crystallisation of the yttrium–sialon glass: Y 15.2 Si 14.7 A l8. 7 O 54.1 N 7.4*, *J. Non. Cryst. Solids.* **270** (2000) 6–19.

[65] ASTM, *Standard Test Methods for Determining Average Grain Size, E112-10, ASTM*, pp. 1–27, 2012.

[66] M. K. Miller and R. G. Forbes, *Atom-probe tomography: the local electrode atom*

probe, 2014.

[67] J. T. Sebastian, *Nanoscale three-dimensional studies of segregation at ceramic/metal interfaces*, PhD thesis, Northwestern University, 2004.

[68] ThermoCalc, "http://www.thermocalc.com/media/8136/tcc_usersguide.pdf." .

[69] B. Kaplan, A. Markström, A. Blomqvist, S. Norgren, and M. Selleby, *Thermodynamic analysis of the Co–Cr–C system*, *Calphad.* **46** (2014) 226–236.

[70] A. Markström, *Thermodynamic modelling of carbides in multicomponent systems: theoretical and experimental approach*, PhD thesis, KTH, 2009.